Nucleation and growth model for {110}- and {111}-truncated nanoparticles

Nicholas J. Jones[a),b)]
Department of Materials Science and Engineering, Carnegie Mellon University, Pittsburgh, Pennsylvania 15213, USA

Raja Swaminathan
Intel Corporation, Chandler, Arizona 85226, USA

Michael E. McHenry[c)] and David E. Laughlin
Department of Materials Science and Engineering, Carnegie Mellon University, Pittsburgh, Pennsylvania 15213, USA

Nanoparticle-sized powders have seen more and more use in many of today's applications. As particle size decreases, many properties change including the ability to embed the small particles in liquids and other media. With decreasing size, however, surface energy becomes more important and can dictate the final shape of the particle. In applications based on polar molecules attaching to the nanoparticle surface, the surface morphology can become a key design parameter. A nucleation and growth model has been constructed for truncated body-centered cubic derivative materials, along with an update to previously published work on face-centered cubic materials. The model shows that for (110)- and (111)-truncations of a cube with a specified surface energy for each surface, the critical nuclei and equilibrium growth shapes are the same, supporting the theory of self-similar growth that had only been mentioned previously, but never proven. In this analysis, saddle points play an important role in determining the critical nuclei for comparison with the equilibrium growth shapes.

I. INTRODUCTION

Nanomaterials research is a growing area that is important for many diverse applications.[1] Solid-state,[2] liquid-phase,[3] and gas-phase[4] nucleation and growth theories are important in understanding nanostructures and controlling their properties. There is a large literature on synthesis → structure → properties → performance relationships in magnetic nanoparticles (MNPs), and the understanding of MNPs relies on studying the increasingly important influence of atoms at surfaces and interfaces, which may contribute differently to properties when compared with atoms in the bulk material. The theory of MNP nucleation and growth can make important contributions to the understanding of MNP morphologies and the resulting properties, which are different from bulk. In this paper we describe the theory of nucleation and growth of (100)- and (110)-faceted surfaces observed in body-centered cubic (BCC) MNPs.

An understanding of the role of surface and interface structure and crystallography on properties of MNPs is an important, evolving area. In face-centered cubic (FCC) derivative nanocrystalline ferrite MNPs, for example, particle morphologies are observed to be faceted with identifiable crystallographic surface orientations.[5–8] It has been demonstrated that these crystallographic orientations lead to distinct magnetic properties for the two different surfaces.[6] The surface morphology is also influential in microstructural development in grain coarsening during sintering.[9]

In BCC FeCo/ferrite core–shell nanoparticles, the core is faceted and orientation relationships between the metal core and oxide shell have been determined (the shell can also be faceted, but only at low thicknesses).[10,11] The surface structure is important in understanding the oxidation process, and the core–shell morphology and terminating surfaces control the functionalization of these materials in a variety of applications.[10,12–14] Explanations for the evolution of nanoparticle morphologies in terms of nucleation and growth models are important for understanding the role of particle morphology

---

on physical properties at different sizes.[1] In this paper, we extend the nucleation and growth models of Ref. 4 to address the observations of (100) and (110) surfaces in FeCo MNPs. The theory of self-similar growth for homogeneous nucleation is also proven, graphically. While this has been investigated for heterogeneous nucleation of precipitates, the homogeneous nucleation of nanoparticles is a simple concept (yet unaddressed in the literature) that has been mentioned, but not proven.[15–17] An analogous 2D model can analytically show that the critical nuclei and equilibrium growth shapes are self-similar, although such a model has not been presented here.

We have calculated both the critical nuclei and equilibrium growth shapes of BCC FeCo MNPs with (100) and/or (110) terminating surfaces by considering the Helmholtz free energies of perfect and truncated cubes and rhombic dodecahedra. This model considers volume and surface energy terms in predicting the critical nucleus shapes. Equilibrium growth shapes are obtained by minimizing the total surface energy associated with (100) and (110) surfaces while constraining the volume to a constant size. Finally, there is a reanalysis of nucleation and growth for FCC-type materials[4] in light of the BCC analysis.

II. REQUIREMENTS FOR NUCLEATION AND EQUILIBRIUM GROWTH SHAPES

In order for a material to nucleate, there is a surface energy barrier that must be overcome. The creation of surfaces, which always *costs* energy, can be considered an introduction of two-dimensional defects. It is for this reason that heterogeneous nucleation is often preferred over homogeneous nucleation, because in heterogeneous nucleation there is already a surface present which can assist in reducing the energy barrier to nucleate new surfaces. Irrespective of the mode of nucleation, the shape of the critical nuclei can be determined to be the nuclei shape that has the lowest free energy of formation. While this has often been thought to be the same as the equilibrium growth shape (often termed "self-similar growth"), this has not been proven analytically for three-dimensional objects.[15]

Beginning very simply, we can look at the general equations for traditional nucleation and growth shown below [Eqs. (1) and (2)].

$$\text{Nucleation} : -V\Delta f_v + \sum \sigma A \quad , \qquad (1)$$

$$\text{Growth} : \sum \sigma A \quad . \qquad (2)$$

The nucleation equation has both a volume energy term and a surface energy term, while the equilibrium growth shape only has a surface energy term. The nucleation equation has a 3rd power volume term, and

a 2nd power surface area term, so we get a traditional nucleation curve, for which the critical nuclei can be found by setting the first derivative equal to zero (finding the critical points), and solving for when the curvature (or second derivative) is less than zero.

While we use the maximum in the nucleation equation to give us the critical nuclei and nucleation energy barrier, we instead find the minimum in energy for the equilibrium growth shape, minimizing the total surface energy. Since we are maximizing in one case and minimizing in another, both with two different equations, it seems reasonable to assume that the shape of the critical nuclei and equilibrium growth shapes will be different, which is contrary to what has been previously stated by Christian and Aaronson.[15,18] This assumption is based upon the traditional arguments using a dimension of the shape, whether that be the radius of a sphere or the edge length of a polyhedra, in a 2D/3D system. It is inadequate, however, to compare edge lengths when dealing with the possibility of different shapes. This will be expanded upon below, with a three-dimensional analysis for both {110} and {111} faceting of cubes, but Fig. 1 shows this graphically for FCC based structures. When plotting the Helmholtz free energy versus the equivalent edge length of multiple polyhedra [Fig. 1(a)], it seems that there is one shape with a minimum nucleation energy barrier (the cube), and another which will provide the minimum energy growth shape at a certain edge length (the cuboctahedron). While this is surely easier to plot, this is misleading and incorrect.

To compare different shapes, we need to compare equivalent volumes, otherwise the energies we are comparing are due to different amounts of atoms attaching to the nucleus, which will alter the energies being compared. By comparing volumes, we remove the volume free energy as a variable and we also change the traditional shape of the nucleation curves [Fig. 1(b)], but we can now do both nucleation and growth analyses at the same time. The minimum energy barrier for nucleation will not change, since we are only transforming the *x*-axis dimensions; we don't change the maxima in energy, but only their lateral position with respect to each other. The size of the critical nucleus doesn't change, but we are using the volume to compare the polyhedra to each other. By comparing volumes, however, we can set a constant volume and compare the energies for the different shapes, which is a Wulff Construction, in essence (rather than removing the volume term from the equation, we are just making it a constant).[19,20] We can now see that the critical nucleus is not different from the equilibrium growth shape but will be the same [Fig. 1(b)], since the curve with the minimum nucleation energy barrier will always be less than any other curve. This is the origin of the difference between this model and the old model,[4] and thus constitutes an improved formalism for self-similar growth.
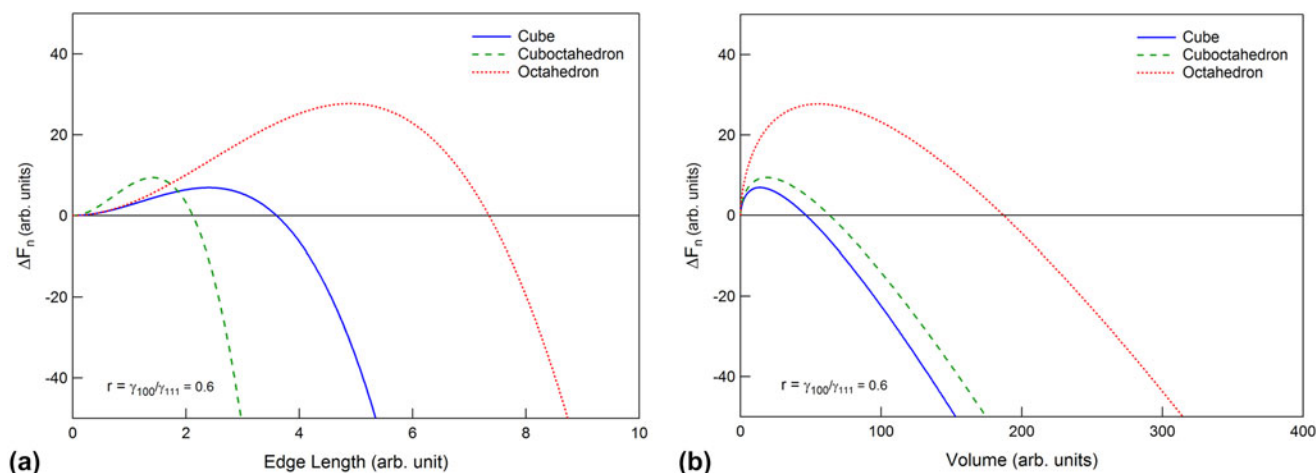
FIG. 1. Helmholtz free energy plots for a cube, cuboctahedron, and octahedron when the FCC surface energy ratio, r, is 0.6, plotted against equivalent edge lengths (a) and equivalent volumes (b).

Instead of choosing three different polyhedra and comparing them, it is better to allow any degree of truncation in a given system (BCC and FCC, in the current paper), and then calculate critical nuclei and equilibrium growth shapes. This is done analytically below, but it is essential to briefly discuss the analysis before continuing. When considering the nucleation of spheres, surface energy is made isotropic, and the calculations only consider critical points in one dimension (the radius). It is therefore only necessary to find the maximum in the nucleation curve. When expanding the two-dimensional graph of *energy* and *shape dimension* to a three-dimensional *energy*, *volume*, and *truncation amount* graph, the surface maximum is no longer of interest. The *volume* axis takes the place of the previous *dimension* axis, and the *truncation* axis allows us to plot all the possible shapes and their energies at one time, starting from no truncation to full truncation (for BCC, cube to rhombic dodecahedron; for FCC, cube to octahedron). We still need to find the maxima along the volume axis, finding the critical nucleus at each truncation ratio. But, while we find the maximum in energy with increasing particle size, we must find the minimum in energy with changing truncation parameter. This is illustrated in Fig. 2, where the two directions of interest are labeled; *edge length* is used for this schematic, rather than *volume* to demonstrate the concept more easily through graphical means, and to preserve the shape of the traditional nucleation curves, but in three-dimensions. While it is not traditionally considered a critical point, this analysis needs to look at *saddle points* as the true minimum in energy, yielding the true critical nucleus and equilibrium growth shapes for a given surface energy ratio between faceting faces.[21]

The saddle figure shown will not always be the shape of the energy surface, due to constraints on the system;

the saddle point may occur at the edges of the plot (i.e., full truncation in either direction). And, in fact, none of the three-dimensional energy surfaces discussed below will look like Fig. 2, completely, since the truncation parameter would need to be plotted logarithmically to show the features accurately in three-dimensions.

III. THREE-DIMENSIONAL MODELS

A. {110} truncations

An in-depth study on the faceting of {100}- and {111}-type faces has already been published, looking at ferrite nanoparticles.[4] FeCo nanoparticles, however, are not based on an FCC crystal structure but rather on a BCC or BCC-derivative structure. Therefore, the faceting planes will be of {100}- and {110}-types, since the {110} planes have the fewest broken bonds; this has been shown for FeCo polydispersed nanoparticles.[10,22] The two basic polyhedra are the cube and the rhombic dodecahedron, represented by only {100} or {110} facets, respectively. The truncated cube and truncated rhombic dodecahedron occupy all shapes in between (see Fig. 3). Similar to the cuboctahedron in Ref. 4, there is a polyhedron in the middle of the truncation for which all the edge lengths are equal. This is termed the truncated rhombic dodecahedron (not to be confused with the rest of the truncated shapes leading up to the rhombic dodecahedron). There is no special name for this polyhedron, though, since the faces are all equilateral, but not regular; the angles of the hexagons are not 120°. This polyhedron, while similar to a truncated octahedron, has only two-fold symmetry for the hexagonal {110} faces.

To begin to quantitatively describe these polyhedra, we need to define dimensions which can describe the area of the {100} and {110} faces, and the volume of the polyhedra. Figure 4 shows the convention used in this
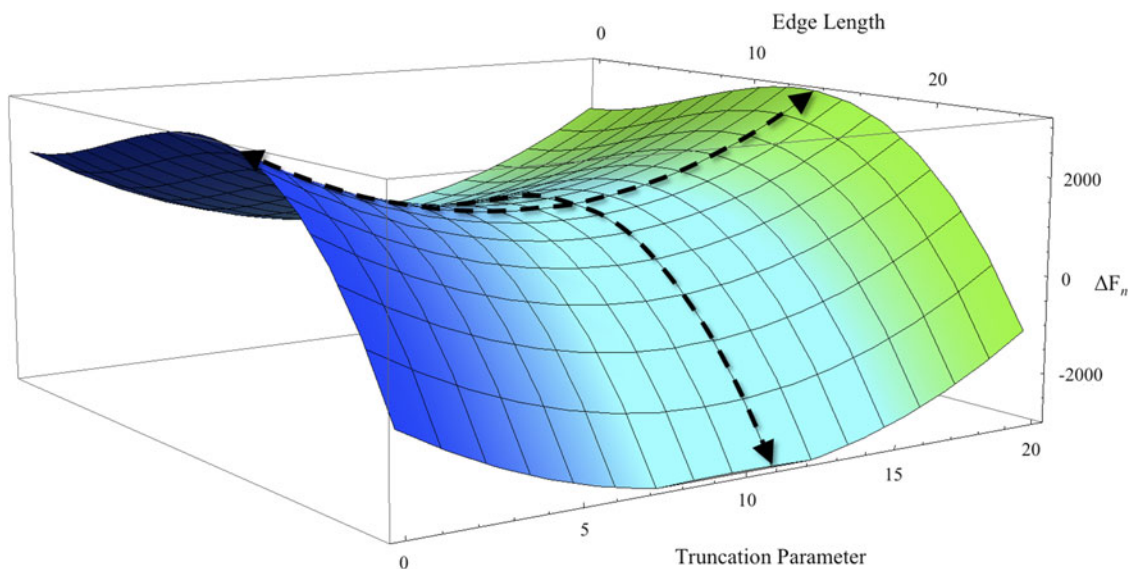
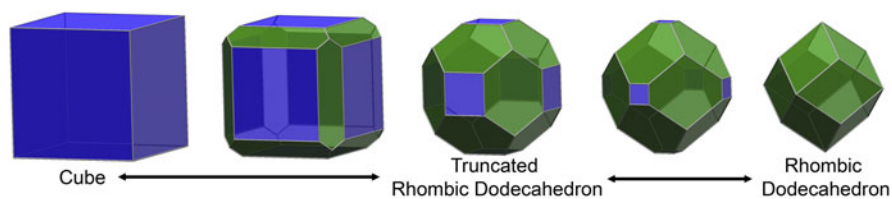FIG. 2. Schematic of a saddle point, illustrating their necessity in free energy critical point analyses.

FIG. 3. Three-dimensional polyhedra progression formed from the {110}-truncation of a cube.

paper. By projecting the shapes in 2-dimesions, we can define x as the edge length of the square, {100} faces, and y as the distance from the end of a {100} face to the next {100} face, projected parallel to the original face ($y\sqrt{2}$ would be the actual distance along the {110} face). In Fig. 4, we see the relationship between lengths a, b, and x, where a is the major length of the rhombic dodecahedron, and b is the truncation parameter parallel to a; x is the edge length of the emerging {100} faces. Cubic parameters, x and y, can be defined for the rhombic dodecahedron, and vice versa, as $x = 2b/\sqrt{3}$ and $y = 2a/\sqrt{3}$.

By combining these different edge-length and truncation parameters, we can get the areas of the {100} and {110} faces and the volumes of the truncated polyhedra, as shown in Table I. As the different polyhedra are truncated, we will have 6 {100} faces and 12 {110} faces that contribute to the overall surface energy of the truncated polyhedra. Because the energy of each face can be different for different materials, the critical nuclei for a certain surface energy ratio can be found by varying the truncation parameters, and the middle equilateral shape can be found when all edge lengths are equal (i.e., $x = a$). This middle shape, however, is not necessarily an equilibrium shape, since that will depend

on the ratio of surface energies. Each of these facets has a different surface energy which we will call γ_{100} and γ_{110}. The bulk energy (free energy of formation of a solid), Δf_v, is independent of shape, and is therefore a constant that can be ignored when comparing the different shape energies. The appropriate equation for calculating the critical nuclei is the Helmholtz free energy of nucleation, given below:

$$\Delta F_n = -V\Delta f_v + 6\gamma_{100} A_{100} + 12\gamma_{110} A_{110} \quad , \quad (3)$$

where all the terms are defined above, and A_{hkl} is the area of an (hkl) face, while V is the volume of the polyhedron. By inputting the equations from Table I, we can get an equation that can be differentiated to find the critical dimensions for nucleation of a certain shape. To simplify these calculations, the free energy of nucleation is normalized by γ_{110}, where $\Delta F_n' = \Delta F_n/\gamma_{110}$ and the ratio of surface energies that can be varied will be $r = \gamma_{100}/\gamma_{110}$. As confirmed by Swaminathan et al., the coefficient in front of the volume term, $\Delta f_v/\gamma_{110}$, can be set to 1 for simplicity; Δf_v for all the shapes will be the same since they have the same crystal structure, and we can assume that γ_{110} is a constant with only γ_{100} varying to produce the different values of r.[4] In contrast to the
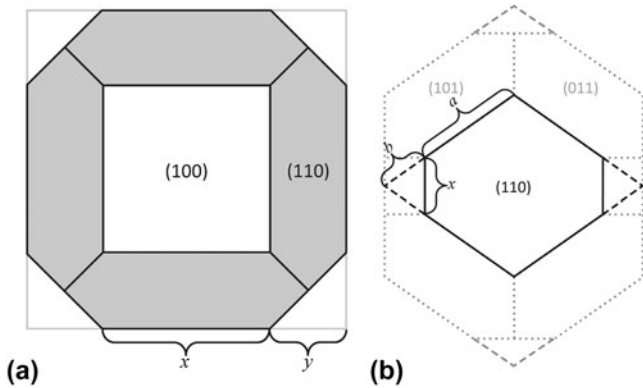
FIG. 4. Projections of the three-dimensional polyhedra formed from the (a) {110}-faceting of a cube and the (b) {100}-faceting of a rhombic dodecahedron, indicating the appropriate measurement lengths for the model.

TABLE I. Volume and area calculations for the various crystallographic facets starting either at the cube or the rhombic dodecahedron.

	Trunc. cube	Trunc. Rh. Dod.
A_{100}	x^2	$(4/3)b^2$
A_{110}	$\sqrt{2}(xy + (y^2/2))$	$2\sqrt{2}/3(2ab + a^2)$
V_T	$x^3 + 6x^2y + 6y^2x + 2y^3$	$8/(3\sqrt{3})(b^3 + 6b^2a + 6a^2b + 2a^3)$

previous work with cubes and octahedra, the equations shown in Table I are continuous between the two end shapes, whereas the FCC shapes could only reach the *cuboctahedron* (a regular polyhedron) continuously; to reach the octahedron, the same facet grows but with none of the original cubic edges remaining. Here, however, no truncation parameter or equation changes are needed to evaluate the nuclei and equilibrium growth shapes for BCC-type polyhedra.

We first proceed to determine the critical nuclei for this system. Let us consider the case of truncating the cube. By differentiating the free energy equations with respect to x, y, a, or b for both the cube and rhombic dodecahedron and setting these new equations equal to zero, we can get the critical points (x_o, y_o, a_o, and b_o) of the curves as a function of r [see Eqs. (4) and (5)].

$$\frac{\partial \Delta F_n'}{\partial x} = -3x^2 - 12xy - 6y^2 + 12rx + 12\sqrt{2}y = 0 \quad , \tag{4}$$

$$\frac{\partial \Delta F_n'}{\partial y} = -6x^2 - 12xy - 6y^2 + 12\sqrt{2}(x + y) = 0 \quad . \tag{5}$$

By solving the system of equations for x and y, the first derivative analysis yields four solutions in terms of r (referred to below as "Cases"). Only the nonnegative

solutions of x and y are applicable, since our polyhedra have to have positive edge lengths. Only the equations for the truncated cube need to be considered, since the rhombic dodecahedron equations are the same equations with substitutions for x and y, and will therefore yield the same results. The first-derivative solutions are summarized below:

(i) $x_o = 0$, $y_o = 0$—trivial case
(ii) $x_o = 0$, $y_o = 2\sqrt{2}$ (rhombic dodecahedron)—nonnegative for all r ranges
(iii) $x_o = 4(\sqrt{2} - r), y_o = -2(\sqrt{2} - 2r)$—nonnegative for $1/\sqrt{2} \le r \le \sqrt{2}$
(iv) $x_o = 4(\sqrt{2} - r), y_o = -4(\sqrt{2} - r)$—nonnegative for $r = \sqrt{2}$ (Trivial).

To understand the nature of these critical points, we can look to the second derivative using combinations of x_o and y_o or a_o and b_o. The second derivative analysis relies upon the use of the Hessian matrix [Eq. (6)] and the following conditions[23,24]:

(i) If $\det(H) > 0$ and $f_{xx}(x_o, y_o) < 0$, then (x_o, y_o) is a local maximum
(ii) If $\det(H) > 0$ and $f_{xx}(x_o, y_o) > 0$, then (x_o, y_o) is a local minimum
(iii) If $\det(H) < 0$, then (x_o, y_o) is a saddle point
(iv) If $\det(H) = 0$, then the second derivative test is inconclusive.

Therefore, a relative maximum in the surface plot occurs when the determinant of the Hessian matrix is positive but $f_{xx}(x_o, y_o)$ or $f_{aa}(a_o, b_o)$ is negative. This traditionally would give us the critical points we need to look at and their valid regions of application.

$$H = \begin{bmatrix} \frac{\partial^2 f}{\partial x^2} & \frac{\partial^2 f}{\partial x \partial y} \\ \frac{\partial^2 f}{\partial y \partial x} & \frac{\partial^2 f}{\partial y^2} \end{bmatrix} \quad or \quad \begin{bmatrix} \frac{\partial^2 f}{\partial a^2} & \frac{\partial^2 f}{\partial a \partial b} \\ \frac{\partial^2 f}{\partial b \partial a} & \frac{\partial^2 f}{\partial b^2} \end{bmatrix} \quad . \tag{6}$$

Following this logic, the second derivative analysis shows that there is no solution that satisfies our requirements for Case 1. Case 2, however, is applicable when $0 \le r \le \sqrt{2}$. This solution does not make conceptual sense, though, since it says that the rhombic dodecahedron is the preferred shape even when the (110) surface energy is infinitely larger than the (100) surface energy. This solution only makes sense above the equality point for the cube and rhombic dodecahedron equations, where the rhombic dodecahedron should be favored. This is found to be at $r = 0.89$, by setting the volumes of the two pure shapes equal to each other, and finding at what surface energy ratio the total energies of the pure shapes are equal too. Case 3 is only applicable when $r = \sqrt{2}$, which reduces to Case 2, and Case 4 has no solution, as expected. The analysis for the rhombic dodecahedron equations yields the same results, since the equations are substitutionally the same.

These solutions, however, are not correct, since the cube is never calculated to be a critical nuclei. Therefore,

it can be assumed that the analysis for this system is not trivial, and is not analogous to the process described by.[4] If the maxima of the x–y plot are found through first and second derivatives and the appropriate use of the Hessian matrix, then there is only one maximum that is found at $x = 0$ and $y = 2\sqrt{2}$, even when the surface energy ratio, r, is 0 (meaning that the γ_{110} energy is infinitely larger than the γ_{100} surface energy); yet, the cubic critical nucleus should be found at least at this extreme. So, further inspection of the curves is needed to understand the appropriate maxima and minima.

By inspecting the equations further, it is not just a maximum in the energy space of x–y that should be considered, but saddle points are also important. A lack of consideration of the saddle points would cause us to miss the *actual* critical nucleus, which is the minimum of all the nucleation energy barriers. There will always be a maximum in the nucleation curve for any shape, yielding a critical nucleus. This maximum can obviously be found by setting the first derivative equal to zero for that shape. However, if we change the shape (meaning the x/a edge-length ratio), we will get a change in the critical nucleus size and energy barrier. By extending this to all possibilities in the x–y plane, we essentially get a series of maxima that line up with each other in polar arrays, which will keep the truncation ratio the same. So if we pick a certain angle in the x–y plane, we have chosen a certain shape and can find the critical nuclei size for the truncation. In combining all these possibilities, however, we want to choose the overall minimum energy barrier to be overcome to nucleate a shape at that desired surface energy ratio, r. As we change that surface energy ratio, the minimum will change, but since we are looking for the minimum in the calculated energy maxima, this point needs to be a saddle point. This is made especially evident when the energies of the rhombic dodecahedron and cube are equal, at $r = 0.89$. It was concluded in Ref. 4 that it is when the energies are equal that the critical nucleus switches from cube to octahedron, or in our case from cube to rhombic dodecahedron. In contrast, this paper posits that this switch does not happen at a single point but rather over a range of points. For BCC polyhedra, this would be continuous from the cube to the rhombic dodecahedron. For the FCC polyhedra, with an intermediate cuboctahedron, there will be two different transitory regions: one region in between the cube and cuboctahedron, and then another transition region between the cuboctahedron and the octahedron. Figure 5 shows the BCC case where $r = 0.89$, and therefore the free-energy of the cube and rhombic dodecahedron are equal. But, as is shown, the energy can still decrease, and it is a minimum at an edge length ratio of $x/a = 3.30963$.

In choosing the saddle point condition for the Hessian matrix ($\det(H) < 0$), a different set of critical points can be found for the transitions between these regions. For
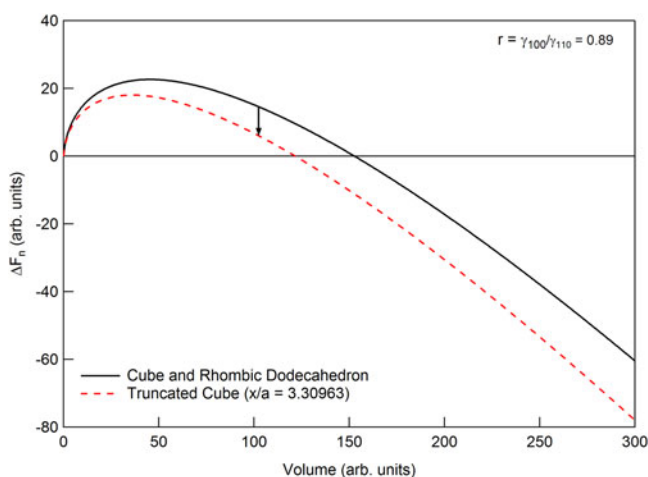

FIG. 5. Helmholtz free-energy of the nucleation of a cube, truncated cube, and rhombic dodecahedron when the surface energy ratio, r, is 0.89, and the free energy of the cube and rhombic dodecahedron are, therefore, equal.

Case 1, the answer is still trivial, although the applicable range is when $0 \leq r < \sqrt{2}$. For Case 2, the rhombic dodecahedron is preferred when $r > \sqrt{2}$. For Case 3, solutions can be found when $1/\sqrt{2} \leq r < \sqrt{2}$, which correspond to variable truncations between the cube and rhombic dodecahedron; at the upper limit, the shape is the rhombic dodecahedron, and at the lower limit the shape is a cube. For Case 4, there are no solutions. The cube is again never mentioned in the solutions above, however, this can be correctly understood by looking at the curves and realizing that the cubic energy minimum is not necessarily at a point when the first derivative is zero, since it is an end-point and therefore cannot truly be evaluated with that requirement; a similar problem exists for the rhombic dodecahedron. If $r \leq 1/\sqrt{2}$, then the critical nuclei are cubes; if $r \geq \sqrt{2}$, then the critical nuclei are rhombic dodecahedra. However, if $1/\sqrt{2} < r < \sqrt{2}$, then it is a truncated shape.

This is the same condition as seen for the equilibrium growth shapes. The equilibrium growth shapes are determined by a minimization of surface energy, which can be calculated by a Wulff construction, where the volume is held constant and only the surface energies are taken into account. While it initially seems necessary to keep the growth shape volume above the critical nuclei size, this is not necessary since the volume only subtracts a constant from all the equations if it is held constant for all polyhedra. By keeping the volume constant, we can see the effect of truncation on the Helmholtz free energy, as depicted in Fig. 6. The volume is set at 1, and the edge lengths x and a are varied in the appropriate ratios to maintain that volume. These curves are almost identical to those that can be shown for surface to volume ratios as a function of truncation. Setting the volume free energy to 1, we can see three regimes of equilibrium growth

shapes with changing r values. At low and high r values, there is a smooth transition in energy between the cube and the rhombic dodecahedron truncations, with the minima lying at the pure shapes in accordance with the r values reported above. At middle values of r, however, the minimum lies at some truncated shape. The two transitions when a truncated critical nucleus becomes and ends being stable are $r = 1/\sqrt{2}$ and $r = \sqrt{2}$, again in accordance with above. Figure 7 shows pictorially the transition regions for critical nuclei and equilibrium growth shapes, and the polyhedra that are stable in each region.

These conclusions agree with the analyses and observations by Wang et al.,[25] Saito et al.,[26] and Hayashi et al.[27] In addition, the particles observed by Jones et al. had similar truncations,[11] resembling particles near the rhombic dodecahedron side of the surface energy ratios (or ratio of growth speed for different planes, as described by Wang et al.). While the nanoparticle techniques used by the former papers produced monodispersed powders where sizes can be varied, the techniques used by Jones et al. produced polydispersed powders with a wide particle size distribution. Those particles produced at high temperatures yielded primarily rhombic dodecahedra or truncated rhombic dodecahedra, while those particles produced at room temperature yielded cubes or truncated cubes. This was attributed by Wang et al. to
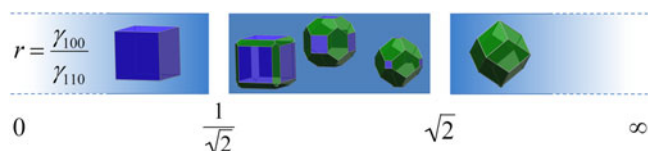
growth kinetics at lower temperatures, which overwhelms the atoms' ability to form the equilibrium shape due to limited atomic motion. It should be noted, therefore, that the morphology of nanoparticles produced during sputtering, gas evaporation, and other nonequilibrium techniques can have a kinetic shape instead of an equilibrium shape. At higher temperatures, however, the atoms have more ability to find their preferred lattice positions and truncation amounts since they are not as constrained to stay in their initial position as determined by the deposition technique. Plasma torch synthesis, therefore, has an interesting possibility to produce many varied shapes and sizes, which depends on where in the argon plasma they nucleate (determining the temperature of nucleation) and the distance remaining for them to grow before reaching temperatures which limit diffusion (determined by the temperature gradient and the nucleation location). This was the basis of the shape changes postulated by Swaminathan et al. for the cube–octahedron cases.[4] Those seen by Jones et al., however, all resemble polyhedra on the side of the rhombic dodecahedra (pure and slightly truncated) or are spherical (as also seen by Wang et al. for the smallest particles).

B. {111} truncations

The cube and octahedron truncations can be analyzed in the same way, and yield slightly different results from those reported previously.[4] For critical nuclei, it was previously shown that the transition between the cube and octahedron occurs at the surface energy ratio of $\gamma_{100}/\gamma_{111} \approx 0.95$. We can see from Fig. 8 that the free energy maxima for these two polyhedra are equal, and if we plot them against volume, both energy curves will be equal. As can be noted, however, the cuboctahedron has a maximum that is lower in energy than both of the assumed critical nuclei; the cuboctahedron, therefore, has a smaller energy barrier that would need to be overcome to nucleate. The cuboctahedron is not actually the lowest energy here, though. The actual preferred shape lies a little further toward the octahedron side. This again prompts a new analysis by utilizing saddle points.

The first derivative analysis for the cube and octahedron truncations is the same as reported previously. In these analyses, a pure cube is defined by only x and a pure octahedron is defined by only x_1. y and y_1 are the truncation parameters for the cube and octahedron, respectively, and are parallel to x and x_1, extending to the original polyhedra vertices.[4] For the cube the first derivative solutions are:

(i) $x = 0$, $y = 0$—trivial case
(ii) $x = 4(\sqrt{3} - 3r)$, $y = -2(\sqrt{3} - 3r)$—nonnegative for $r = 1/\sqrt{3}$ (Trivial)
(iii) $x = 4(\sqrt{3} - 2r)$, $y = -2(\sqrt{3} - 3r)$—nonnegative for $1/\sqrt{3} \leq r \leq \sqrt{3}/2$
(iv) $x = 4r$, $y = 0$ (cube)—nonnegative for all r ($r \geq 0$).
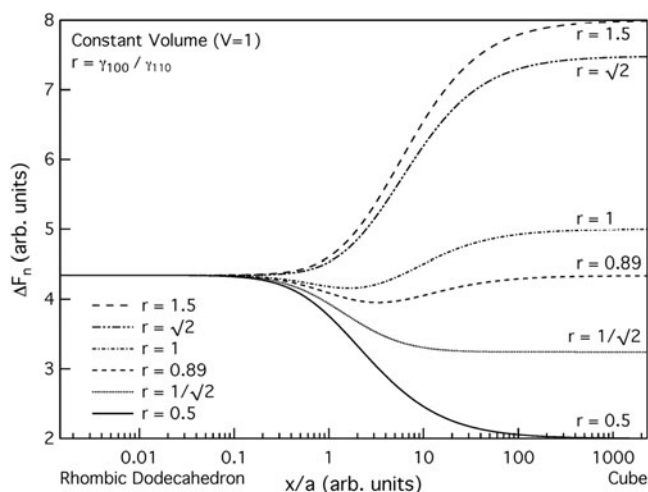

FIG. 6. A plot of the free energy of nucleation versus truncation parameter for BCC materials (at constant volume).

FIG. 7. The critical points of the surface energy ratio, r, for both the critical nuclei and the equilibrium growth shapes of BCC materials.
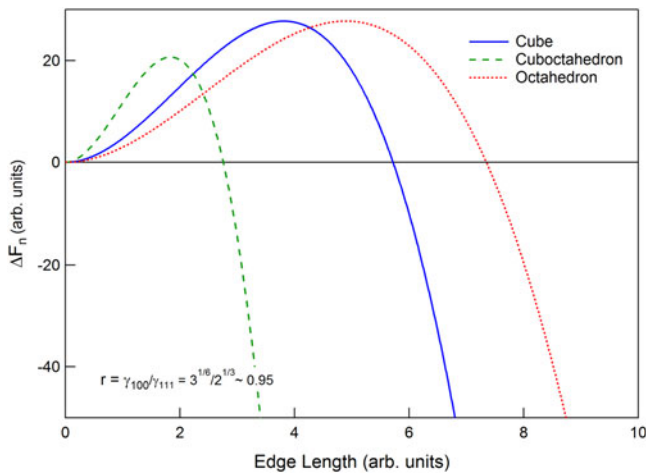
FIG. 8. Helmholtz free-energy of nucleation of a cube, cuboctahedron, and octahedron when the surface energy ratio, r, is $\gamma_{100}/\gamma_{111} = 3^{1/6}/2^{1/3} \approx 0.95$.

For the octahedron, they are:

(i) $x_1 = 0$, $y_1 = 0$—trivial case

(ii) $x_1 = 2\sqrt{6}$, $y_1 = 0$ (octahedron)—nonnegative for all r

(iii) $x_1 = -2(\sqrt{6} - 2\sqrt{2}r)$, $y_1 = 2(\sqrt{6} - \sqrt{2}r)$—nonnegative for $\sqrt{3}/2 \leq r \leq \sqrt{3}$

(iv) $x_1 = -4(\sqrt{6} - \sqrt{2}r)$, $y_1 = 2(\sqrt{6} - \sqrt{2}r)$—nonnegative for $r = \sqrt{3}$ (Trivial).

The second derivative analysis yields different critical nuclei than those reported by Swaminathan et al. due to the criterion of saddle points, rather than maxima. For the cube, we will ignore Case 1, since this does not correspond to any polyhedra. Case 2 also corresponds to no polyhedra. Case 3 is applicable when $1/\sqrt{3} \leq r \leq \sqrt{3}/2$, and Case 4 is applicable when $0 < r < 1/\sqrt{3}$. So, for the range of Case 4 we will get the cube, and for Case 3, we will have a truncated shape, ending with the cuboctahedron at $\sqrt{3}/2$. The transition between the cube and truncated cubes begins at $1/\sqrt{3}$, which is why neither shape is solely applicable at that r value.

For the octahedron equations, we will again ignore Case 1. Case 2 corresponds to an octahedron and is applicable when $r > \sqrt{3}$. Case 3 is applicable when $\sqrt{3}/2 \leq r \leq \sqrt{3}$, corresponding to truncated octahedra, and ending with the cuboctahedron at $\sqrt{3}/2$. Case 4 is not applicable to polyhedra. So, again we see that the transition between truncated and pure shapes $(r = \sqrt{3})$ could correspond to either shape, since that is the transition point. And, all polyhedra meet at $r = \sqrt{3}/2$, where the cuboctahedron connects the two sets of equations and truncations. This intermediate shape is only stable at one point, but is necessary since the truncation parameters need to change when we get to this Archimedean solid. This is not necessary in the {110} case above since there is no intermediate Archimedian solid.
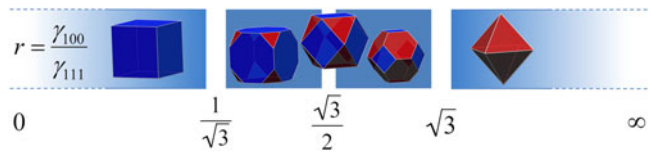

FIG. 9. The critical points of the surface energy ratio, r, for both the critical nuclei and the equilibrium growth shapes of FCC materials.

These answers make more conceptual sense than those reported previously, where there was an overlapped region of cube and octahedron critical nuclei. Here, however, it is well defined that when r is less than $1/\sqrt{3}$ we will have a pure cube nucleate. When r is between $1/\sqrt{3}$ and $\sqrt{3}$, we will observe continuous truncation shapes between the cube and octahedron, with an intermediate cuboctahedron at $r = \sqrt{3}/2$. Above $r = \sqrt{3}$, the octahedron will be the critical nucleus (see Fig. 9). It is comforting to note that the cutoffs for this system are determined by $\sqrt{3}$, since these are dealing with truncations with a normal along the cubic body diagonal, and the previous system was determined by $\sqrt{2}$, since that system was concerned with truncation normals along the face diagonals. In both cases, the equilibrium growth shapes are the same as the critical nuclei, and when the free energy is plotted against volume, rather than truncation parameter, this can be observed. As was noted above, the critical nuclei for $r = 3^{1/6}/2^{1/3}$ is a truncated octahedra, which is slightly less truncated than the cuboctahedron. This is in agreement with the second derivative analysis, since $3^{1/6}/2^{1/3}$ is larger than $\sqrt{3}/2$, which puts it in the truncated octahedron regime.

IV. CONCLUSION

It has been shown that critical nuclei and equilibrium growth particles have the same polyhedra, and therefore proceed through self-similar growth, as was previously postulated but not proven. This verification relies upon a graphical analysis comparing the volume of shapes, rather than edge lengths as is normally done when assuming spherical particles. The analysis of critical nuclei utilizes saddle points to find the critical edge length parameters, which combine the search for an energy barrier (local maximum) for a certain particle shape, with the finding of the minimum energy barrier by comparing the nucleation barrier for all possible polyhedra for that crystal structure. This analysis relies primarily upon the surface energy ratio, and not any volumetric considerations.

The critical polyhedra proceed continuously from one pure shape to another pure shape (fully truncated) with changing surface energy ratio, with no intermediate shape taking any precedence through the transition. For BCC polyhedra, this proceeds from a cube (for $r \leq \sqrt{2}/2$)

through all (110)-truncations ($\sqrt{2}/2 \leq r \leq \sqrt{2}$) until the rhombic dodecahedron ($r \geq \sqrt{2}$). In the case of FCC polyhedra, the cuboctahedron only holds a transitionary place due to the necessity of changing calculation parameters, when the original edge lengths no longer exist. It is, however, just a stopping point for analytical purposes, and nothing more (even though it is an Archimedean solid). The FCC solids proceed from cube (for $r \leq \sqrt{3}/3$) through all (111)-truncations $\left(\sqrt{3}/3 \leq r \leq \sqrt{3}\right)$ until the octahedron $\left(r \geq \sqrt{3}\right)$.

ACKNOWLEDGMENTS

REFERENCES

1. M.E. McHenry and D.E. Laughlin: Nano-scale materials development for future magnetic applications. *Acta Mater.* **48**, 223 (2000).
2. P.R. Ohodnicki, Jr., D.E. Laughlin, M.E. McHenry, and M. Widom: Application of classical nucleation theory to phase selection and composition of nucleated nanocrystals during crystallization of Co-rich (Co,Fe)-based amorphous precursors. *Acta Mater.* **58**, 4804–4813 (2010).
3. K.L. McNerny, Y. Kim, D.E. Laughlin, and M.E. McHenry: Synthesis of monodisperse γ-Fe–Ni magnetic nanoparticles with tunable Curie temperatures for self-regulated hyperthermia. *J. Appl. Phys.* **107**, 09A312 (2010).
4. R. Swaminathan, M.A. Willard, and M.E. McHenry: Experimental observations and nucleation and growth theory of polyhedral magnetic ferrite nanoparticles synthesized using an RF plasma torch. *Acta Mater.* **54**, 807–816 (2006).
5. S. Son, R. Swaminathan, and M.E. McHenry: Structure and magnetic properties of thermally plasma synthesized Mn and Mn–Zn ferrite nanoparticles. *J. Appl. Phys.* **93**, 7495–7497 (2003).
6. R. Swaminathan, M.E. McHenry, P. Poddar, and H. Srikanth: Magnetic properties of polydisperse and monodisperse NiZn ferrite nanoparticles interpreted in a surface structure model. *J. Appl. Phys.* **97**, 10G104 (2005).
7. R. Swaminathan and M.E. McHenry, S. Calvin, M. Sorescu, and L. Diamandescu: Surface structure model of cuboctahedrally truncated ferrite nanoparticles: Properties of nanostructured ferrites. In *Proceedings of the 9th International Conference on Ferrites, San Francisco, CA, USA*, R.F. Soohoo eds.; Wiley-Blackwell, Hoboken, NJ, 2005; pp. 847–852.
8. R. Swaminathan, N.T. Nuhfer, and M.E. McHenry: 3-dimensional morphologies of truncated ferrite nanoparticles. *Microsc. Microanal.* **11**(Suppl. 02), 1904–1905 (2005).
9. R. Swaminathan, J. Woods, S. Calvin, J. Huth, and M.E. McHenry: Microstructural evolution model of the sintering behavior and magnetic properties of NiZn ferrite nanoparticles. *Adv. Sci. Technol.* **45**, 2337–2344 (2006).
10. K.N. Collier, N.J. Jones, K.J. Miller, Y. Qin, D.E. Laughlin, and M.E. McHenry: Controlled oxidation of FeCo magnetic nanoparticles to produce faceted FeCo/ferrite nanocomposites for rf heating applications. *J. Appl. Phys.* **105**, 07A328 (2009).
11. N.J. Jones, K.L. McNerny, A.T. Wise, M. Sorescu, M.E. McHenry, and D.E. Laughlin: Observations of oxidation mechanisms and kinetics in facetted FeCo nanoparticles. *J. Appl. Phys.* **107**, 09A304 (2010).
12. A.H. Habib, C.L. Ondeck, P. Chaudhary, M.R. Bockstaller, and M.E. McHenry: Evaluation of iron-cobalt/ferrite core-shell nanoparticles for cancer thermotherapy. *J. Appl. Phys.* **103**, 07A307 (2008).
13. K.J. Miller, H.B. Soll-Morris, K.N. Collier, R. Swaminathan, and M.E. McHenry: Induction heating of FeCo nanoparticles for rapid RF curing of epoxy composites. *J. Appl. Phys.* **105**, 07E714 (2009).
14. A.H. Habib, M.G. Ondeck, K.J. Miller, R. Swaminathan, and M.E. McHenry: Novel solder-magnetic particle composites, their reflow using AC magnetic fields. *IEEE Trans. Magn.* **46**, 2187–2190 (2010).
15. J.W. Christian: *The Theory of Transformations in Metals and Alloys, Part 1: Equilibrium and General Kinetic Theory*, 2nd ed. (Pergamon Press, New York, NY, USA, 1975); p. 437.
16. Z. Erdélyi, Z. Balogh, and D.L. Beke: Kinetic critical radius in nucleation and growth processes—Trapping effect. *Acta Mater.* **58**(17), 5639–5645 (2010).
17. L. Zhang, L.Q. Chen, and Q. Du: Simultaneous prediction of morphologies of a critical nucleus and an equilibrium precipitate in solids. *Commun. Comput. Phys.* **7**, 674–682 (2010).
18. H.I. Aaronson and J.K. Lee: The kinetic equations of solid → solid nucleation theory and comparisons with experimental observations. In *Lectures on the Theory of Phase Transformations*, 2nd ed., H.I. Aaronson ed.; The Minerals, Metals & Materials Society: Warrendale, PA, USA, 1975; pp. 178–179.
19. C.A. Johnson: Generalization of the Gibbs–Thomson equation. *Surf. Sci.* **3**(5), 429–444 (1965).
20. G. Wulff: XXV. Zur Frage der Geschwindigkeit des Wachsthums und der Auflösung der Krystallflächen. *Zeit. f. Krist.* **34**, 449 (1901).
21. V. Raghavan: *Solid State Phase Transformations* (Prentice-Hall of India Private limited, Connaught Circus, New Delhi, India, 1992); pp. 60–61.
22. J.K. Mackenzie, A.J.W. Moore, and J.F. Nicholas: Bonds broken at atomically flat crystal surfaces—I. *J. Phys. Chem. Solids* **23**, 185–196 (1962).
23. I.S. Gradshteyn and I.M. Ryzhik: *Table of Integrals, Series and Products*, 7th ed., A. Jeffrey and D. Zwillinger eds.; Elsevier, Inc.: Burlington, MA, USA, 2007; p. 1079.
24. J. Stewart: *Calculus: Early Transcendentals*, 5th ed. (Thomas Learning, Inc., Belmont, CA, USA, 2003); p. 954.
25. C.M. Wang, D.R. Baer, J.E. Amonette, M.H. Engelhard, Y. Qiang, and J. Antony: Morphology and oxide shell structure of iron nanoparticles grown by sputter-gas-aggregation. *Nanotechnology* **18**, 255603 (2007).
26. Y. Saito, K. Mihama, and R. Uyeda: Formation of ultrafine metal particles by gas-evaporation: VI. Bcc metals, Fe, V, Nb, Ta, Cr, Mo and W. *Jpn. J. Appl. Phys.* **19**(9), 1603–1610 (1980).
27. T. Hayashi, T. Ohno, S. Yatsuya, and R. Uyeda: Formation of ultrafine metal particles by gas-evaporation technique. IV. Crystal habits of iron and Fcc metals, Al, Co, Ni, Cu, Pd, Ag, In, Au and Pb. *Jpn. J. Appl. Phys.* **16**(5), 705–717 (1977).